Magnetic domain wall neuron with lateral inhibition

Journal of Applied Physics

Magnetic domain wall neuron with lateral inhibition

Cite as: J. Appl. Phys. **124**, 152127 (2018); https://doi.org/10.1063/1.5042452
Submitted: 31 May 2018 . Accepted: 15 September 2018 . Published Online: 09 October 2018

Naimul Hassan, Xuan Hu, Lucian Jiang-Wei, Wesley H. Brigner, Otitoaleke G. Akinola, Felipe Garcia-Sanchez, Massimo Pasquale, Christopher H. Bennett, Jean Anne C. Incorvia, and Joseph S. Friedman

JOURNAL OF APPLIED PHYSICS **124**, 152127 (2018)

Magnetic domain wall neuron with lateral inhibition

Naimul Hassan,[1,a)] Xuan Hu,[1,a)] Lucian Jiang-Wei,[1] Wesley H. Brigner,[1] Otitoaleke G. Akinola,[2] Felipe Garcia-Sanchez,[3] Massimo Pasquale,[3] Christopher H. Bennett,[4] Jean Anne C. Incorvia,[2] and Joseph S. Friedman[1,b)]

[1]*Department of Electrical and Computer Engineering, The University of Texas at Dallas, 800 W. Campbell Rd., Richardson, Texas 75080, USA*

[2]*Department of Electrical and Computer Engineering, The University of Texas at Austin, 2501 Speedway, Austin, Texas 78712, USA*

[3]*Istituto Nazionale di Ricerca Metrologica, Strada delle Cacce, 91, Torino 10135, Italy*

[4]*Centre de Nanosciences et de Nanotechnologies, Université Paris-Saclay, 220 rue André Ampère, Orsay 91405, France*

(Received 31 May 2018; accepted 15 September 2018; published online 9 October 2018)

The development of an efficient neuromorphic computing system requires the use of nanodevices that intrinsically emulate the biological behavior of neurons and synapses. While numerous artificial synapses have been shown to store weights in a manner analogous to biological synapses, the challenge of developing an artificial neuron is impeded by the necessity to include leaking, integrating, firing, and lateral inhibition features. In particular, previous proposals for artificial neurons have required the use of external circuits to perform lateral inhibition, thereby decreasing the efficiency of the resulting neuromorphic computing system. This work therefore proposes a leaky integrate-and-fire neuron that intrinsically provides lateral inhibition, without requiring any additional circuitry. The proposed neuron is based on the previously proposed domain-wall magnetic tunnel junction devices, which have been proposed as artificial synapses and experimentally demonstrated for non-volatile logic. Single-neuron micromagnetic simulations are provided that demonstrate the ability of this neuron to implement the required leaking, integrating, and firing. These simulations are then extended to pairs of adjacent neurons to demonstrate, for the first time, lateral inhibition between neighboring artificial neurons. Finally, this intrinsic lateral inhibition is applied to a ten-neuron crossbar structure and trained to identify handwritten digits and shown via direct large-scale micromagnetic simulation for 100 digits to correctly identify the proper signal for 94% of the digits. *Published by AIP Publishing.* https://doi.org/10.1063/1.5042452

I. INTRODUCTION

Whereas conventional computing machines efficiently solve staggeringly difficult deterministic problems, the human brain is far superior for processing unstructured real-world information. Furthermore, the accomplishment of some tasks, such as those related to pattern recognition, can be achieved by the human brain with orders-of-magnitude less energy than with a computer.[1–3] Though human understanding of our own mental processes is far from complete, neuroscience researchers have identified neurons and synapses as core elements of our neural information processing systems: the neurons emit electrical signals based on input electrical signals, while the synapses provide electrical connectivity between the neurons. These electrical interactions are generally responses to external stimuli and result in changes to the physical state of a person through modifications of memory, hormonal changes, and physical actions (e.g., talking, walking). It is generally believed that these external stimuli cause short- and long-term changes to the synapses, temporarily or permanently modifying the connectivity between neurons.[4] By modifying the connectivity between neurons, the brain responds to external stimuli by altering the circuit through which external stimuli cause changes in the human's physical state. Simultaneously, the brain also responds to these external stimuli by taking the actions prescribed by the circuit.

In order to realize an efficient artificial neuromorphic information processing system, the system should be designed specifically to emulate the electrical interactions present within a biological system. While much previous work has involved software simulation of neurons and synapses with general purpose computing hardware,[5–7] the energy consumed by these systems exceeds that of the brain by orders of magnitude.[8,9] Efforts are therefore underway to develop a neuromorphic hardware system, with exciting recent results achieved with silicon transistor circuits that emulate the behavior of both neurons and synapses.[10–12] However, as silicon transistors inherently provide volatile binary switching that does not readily map to neuron and synapse behavior, it is expected that the use of nanodevices that emulate neuron and synapse behavior will drastically increase the efficiency of neuromorphic computing systems. The non-volatility provided by spintronic devices, as well as memristors, is particularly promising for the development of nanodevices that intrinsically emulate neurological behavior.

[a)]N. Hassan and X. Hu contributed equally to this work.
[b)]Author to whom correspondence should be addressed: joseph.friedman@utdallas.edu.

While numerous two-terminal nanodevices[13]—particularly memristors[14,15]—have been shown to modulate the resistance in a non-volatile manner analogous to the behavior of biological synapses, the relative complexity of neuron functionality has impeded the identification of analogous behavior in nanodevices.[16–18] In particular, neuroscientific studies suggest that biological neurons integrate input signals over time and fire once a threshold value has been reached.[19] In the absence of a strong input, the neurons leak over time and eventually reset to a relaxed state. Furthermore, neighboring neurons interact in an inhibitory manner via a variety of species of connected inhibitory interneurons.[20] These interneurons utilize neurotransmitter projections [i.e., γ-aminobutyric acid (GABA)] to continuously reduce the effectiveness of neighbors by altering the synaptic efficiency of contributing synapses or directly preventing depolarization.[21,22]

As the nature of firing requires the interaction of external devices and therefore must be implemented in concert with an external circuit, the ideal artificial neuron should inherently perform leaking, integration, and lateral inhibition. Several spintronic neurons have been proposed,[23–28] including spiking neurons[23,29] that inherently perform integration. However, these neurons require complementary hardware to perform leaking and lateral inhibition. Furthermore, lateral inhibition has been demonstrated in spintronic neurons through the use of an additional crossbar row.[29–31]

This paper therefore proposes the first artificial neuron that inherently performs integrating, leaking, and lateral inhibition within a single nanodevice. This is achieved by adapting the experimentally-proven[32] domain wall-magnetic tunnel junction (DWMTJ) device,[33] which has heretofore been applied to Boolean logic,[32–34] artificial synapses,[25,26,35–37] and artificial neurons that intrinsically provide neither leaking nor lateral inhibition.[25,26,31] By adding a hard ferromagnet below the DWMTJ track to cause behavior analogous to leaking, a novel device is here demonstrated with micromagnetic simulation to intrinsically perform the leaking, integration, and lateral inhibition required by an artificial neuron. Similar to previous work,[28,38] firing is achieved in concert with an external circuit when the MTJ resistance is switched by the propagation of a domain wall within the soft ferromagnetic track. The ferromagnetic tracks create stray fields that inhibit the motion of domain walls within the ferromagnetic tracks of adjacent neurons, thus inherently providing lateral inhibition. The efficacy of this approach within a large system is demonstrated with micromagnetic simulations of a winner-take-all (WTA) output neuron layer that achieve an accuracy of 94% for the well-known task of handwritten digit recognition.

II. BACKGROUND

The development of a hardware neural network requires artificial neurons and synapses that intrinsically function in a manner analogous to their biological analogs. In order to enable fabrication that is compatible with conventional processes, a synapse crossbar array connects the neurons. In order to emulate biological processes and implement the winner-take-all schemes involved in many machine learning techniques, these neurons must provide lateral inhibition, which is achieved here by adapting the DW-MTJ device.

A. Leaky integrate-and-fire neuron

The leaky integrate-and-fire (LIF) neuron has been well-established as a primary area of interest for the development of an artificial neuron and is a modified version of the original integrate-and-fire circuit.[39] It is based on the biological neuron, which operates in a network of other neurons, communicating via electrical spikes and chemical signals. In order to emulate this method of communication, an electrical LIF neuron sends spikes of voltage periodically, resulting from input currents arriving through synapses connected to other neurons in the network. In addition, there is also a refractory period, in which a neuron cannot fire for a certain amount of time after it has recently fired.

An LIF neuron continually integrates the energy provided by an input current until a threshold is reached and the neuron fires, emitting this energy as a voltage spike that provides current to other neurons via synapse connections. By emitting this energy, the neuron is returned to a low energy state and continues to integrate input current until its next firing. Throughout this process, the energy stored in the neuron continually leaks such that if insufficient input current is provided, the neuron gradually reverts to a low energy state. This prevents the device from indefinitely retaining energy, which would not match the behavior of biological neurons. The LIF behavior is illustrated in Fig. 1, where an input current continually modulates the energy (stored as voltage) within a LIF neuron. A large current is continually applied during the initial stage, resulting in repeated periods of integration interrupted by firing events. When no current is applied, the neuron leaks energy by decreasing the stored voltage.

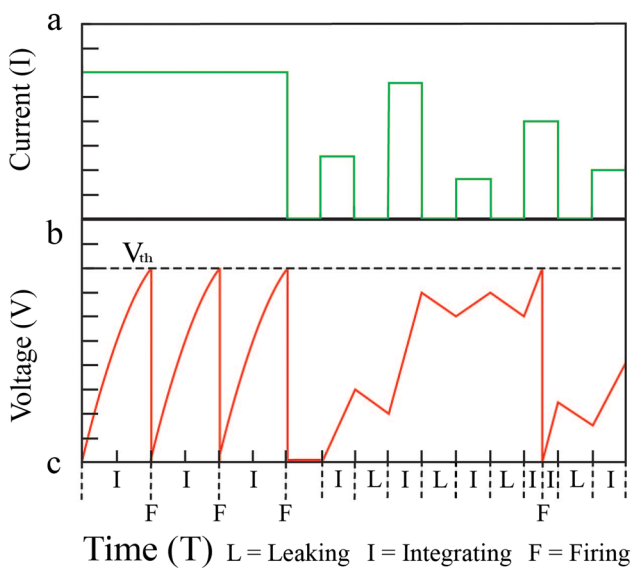

FIG. 1. The leaking, integrating, and firing of a leaky integrate-and-fire neuron. The input current shown in (a) causes leaking, integrating, and firing, as noted in (b). (c) Shows the labels of the three phases that the leaky integrate-and-fire can go through when excited by the input current.

B. Synapse

In biological systems, the synapse is the gap between two neurons and acts as a passageway of communication between the two by sending and receiving information via neurotransmitters on either end of each neuron. In neuromorphic computing architectures, synapses play a similar role, where each synapse has a resistance that determines the current provided to output neurons based on the voltage applied to the input neurons. The connectivity is defined by an internal weight that is refined while training to enable the processing of particular types of data.

Artificial synapses are a key component of neuromorphic computing systems, and the DW-MTJ has previously been shown as an intriguing spintronic synapse.[25,26,36] The non-volatility of the DW-MTJ and other proposed synapses[16–18] enables low energy consumption.[40] Furthermore, the potential use of a single device type for both synapses and neurons is highly advantageous for the development of an integrated neuromorphic system.

C. Crossbar array

Crossbar arrays enable the area-efficient integration of many devices that can be connected to vertical and horizontal wires. Similar to those frequently used in memory, many neuromorphic crossbar arrays incorporate memristors at each intersection in the array. As can be seen from Fig. 2, a synapse sits at each crosspoint of the array, determining the strength of the connection between one input neuron and one output neuron. Though Fig. 2 shows an 8×8 crossbar, it should be noted that the size of a crossbar array can be varied and that the structure need not be square.

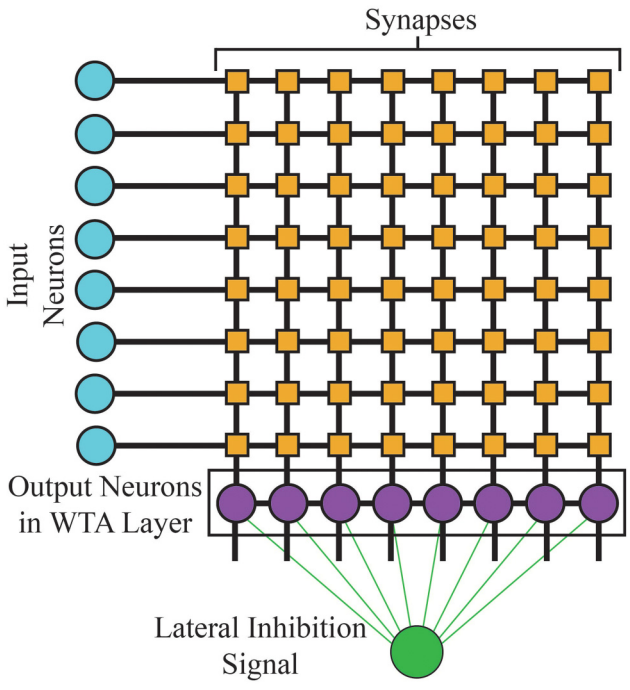

FIG. 2. Neuromorphic crossbar array. The output neurons are connected in a winner-take-all (WTA) manner such that only one output neuron is able to fire within a given time period.

D. Lateral inhibition and winner-take-all

Lateral inhibition is a process that allows an excited neuron to inhibit, or reduce, the activity of other nearby or connected neurons.[41,42] One such neural computing system that seeks to take advantage of this is the winner-take-all system.[43,44] As a form of competitive learning, artificial neurons contend for activation, meaning that only one neuron is chosen as the winner and allowed to fire, using lateral inhibition to suppress the output of all other neurons. After the winning neuron fires, the system is reset and the neurons once again compete for activation. A winner-take-all system is one of the many machine learning paradigms that take advantage of the lateral inhibition phenomenon, which is commonly used in recognition and modeling processes.

In Fig. 2, the output neurons are arranged in a winner-take-all configuration. Depending on the input currents from the input neurons and the weights stored in the crossbar synapses, one output neuron is chosen to fire. As all output neurons are connected, the firing of the winning neuron prevents the firing of the other neurons through lateral inhibition. After the winning neuron fires, the external node emits an inhibitory signal, resetting the whole system.

E. Domain wall-magnetic tunnel junction

The DW-MTJ device[32,33] consists of a soft ferromagnetic track within which a magnetic DW moves, antiferromagnets at both ends to contain the DW within the track, and a MTJ that is in either a high or low resistance state depending on the position of the DW in relation to the MTJ. [This device is similar to that of Fig. 3(a), though without the hard ferromagnet beneath the soft ferromagnetic track.] When sufficient current flows through the DW track, a torque is induced on the DW that causes it to move in the direction of electron motion. Alternatively, spin-orbit torque[45,46] can be used to provide increased efficiency; the general device behavior would be unchanged.

The DW-MTJ has previously been demonstrated experimentally and can be used to perform logical operations[32–34] as well as to implement artificial synapses[25,26,35–37] and neurons.[25,26,31] These functions are performed by selective use of the three terminals of the device: writing is performed by applying a voltage between the two antiferromagnets such that the current flows through the track to move the DW; reading is performed by applying voltage between the MTJ and either side of the device such that the resulting current is dependent on the position of the DW relative to the MTJ.

III. LEAKY INTEGRATE-AND-FIRE DOMAIN WALL NEURON

By adding a hard ferromagnet below the DW-MTJ described above, the DW-MTJ functions as a leaky integrate-and-fire neuron. The application of current causes the DW to shift within the track for integration, the nearby hard ferromagnet causes the DW to shift in the opposite direction for leaking, and firing occurs when the DW passes beneath the MTJ. In addition, magnetostatic coupling between adjacent neurons provides the lateral inhibitory

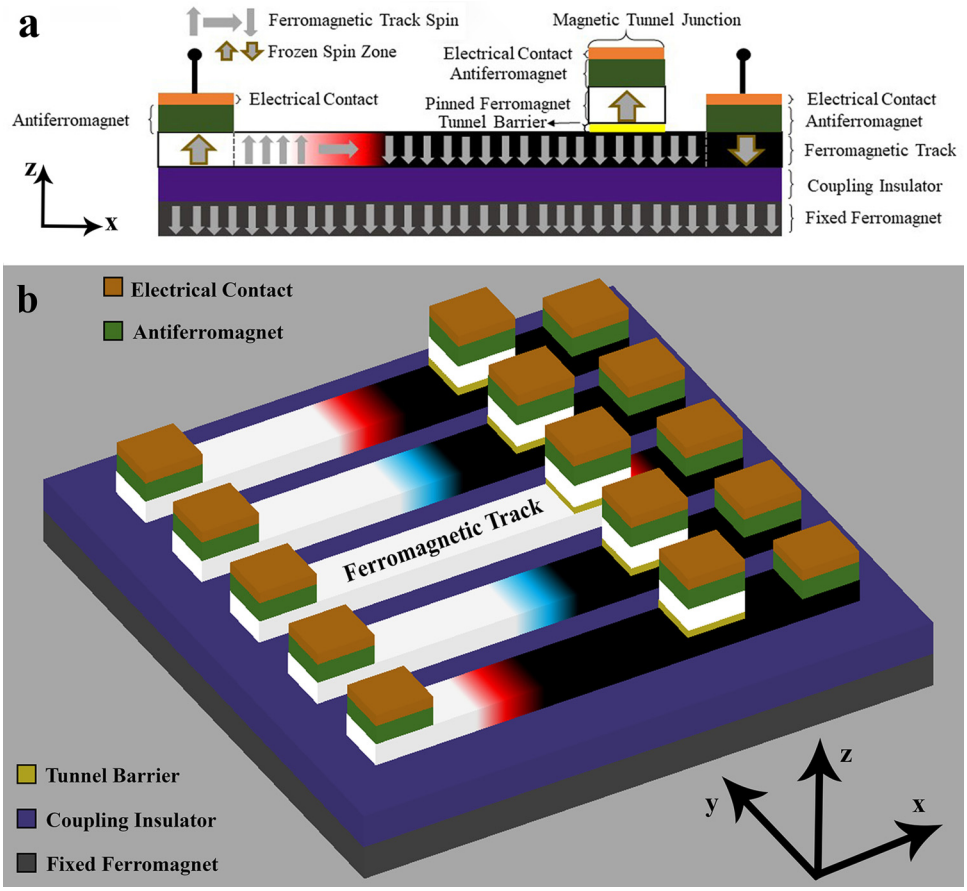

FIG. 3. (a) The DW-MTJ neuron is composed of a ferromagnetic track containing a DW. A fixed ferromagnet provides a constant magnetic field to cause leaking, while current between the two electrical contacts causes integration. When the DW traverses the MTJ, the resistance changes causing the firing of an output spike. (b) For multiple neighboring neurons, a shared fixed ferromagnet provides an identical leaking field to all neurons. In this figure, the central neuron is firing.

behavior which is critically important for the implementation of neural networks. The intrinsic lateral inhibition—without any peripheral overhead circuitry—enables the design of compact and energy-efficient neurons.

A. Device structure

As shown in Fig. 3(a), the neuron consists of the DW-MTJ[32,33] with the addition of a hard ferromagnetic layer beneath the neuron. A conductive ferromagnet or an insulating ferrimagnet can be used, which could be sputter deposited *in situ* with the other thin film layers. The bottom magnet stray field affects the DW through an insulating coupling layer whose thickness can be chosen to optimize the proximity field.

The DW track modeled for this device is 600 nm, 32 nm, and 1.5 nm in the x-, y-, and z-directions, respectively. The track has perpendicular magnetic anisotropy: it is magnetized in the $+z$ direction to the left of the DW and in the $-z$ direction to the right of the DW. The DW magnetization itself rotates in the x-y plane. At either end of the track, the antiferromagnets create regions of constant magnetization through exchange bias that are modeled in micromagnetic simulation by 30 nm-wide regions of frozen magnetic spins. Therefore, the DW is capable of moving within a 540 nm range in the track. The results described in the remainder of this work are based on Mumax3[47] simulations with the following magnetic parameters: saturation field value of 1 T, exchange stiffness of 13×10^{-12} J/m, perpendicular anisotropy constant of 4×10^5 J/m^3, polarization of spin transfer torque of 1, non-adiabaticity factor of 0.9, Landau-Lifshitz damping constant of 0.015, and discretization cell size of $1 \times 1 \times 1$ nm^3.

B. Leaking

The leaking functionality is implemented by a 20 mT magnetic field produced by a ferromagnet beneath the DW track in the $-z$ direction. This produces a constant force that results in the DW shifting in the $-x$ direction. In the absence of current and under the sole influence of the magnetic field, the DW shifts in the $-x$ direction as can be seen from Fig. 4 and the accompanying multimedia view. This oscillatory DW motion is a result of precession of the DW under the magnetic field. In the absence of an applied current, the DW traverses the entire available track in around 220 ns, which corresponds to an average velocity of 2.5 m/s.

A primary advantage of this leaking technique is that no external excitations are required to drive the leaking mechanism: the hard ferromagnet beneath the DW track continuously provides the required magnetic field. Whereas other proposed neuron leaking schemes require the use of a small leaking current flowing through the neuron that results in resistive power dissipation,[29,30] our proposed leaking scheme avoids this power dissipation by replacing the leaking current with a constant magnetic field. Furthermore, as no external excitations must be applied by an external control circuit to perform leaking, the proposed leaking scheme avoids the hardware costs associated with overhead circuits.[48]

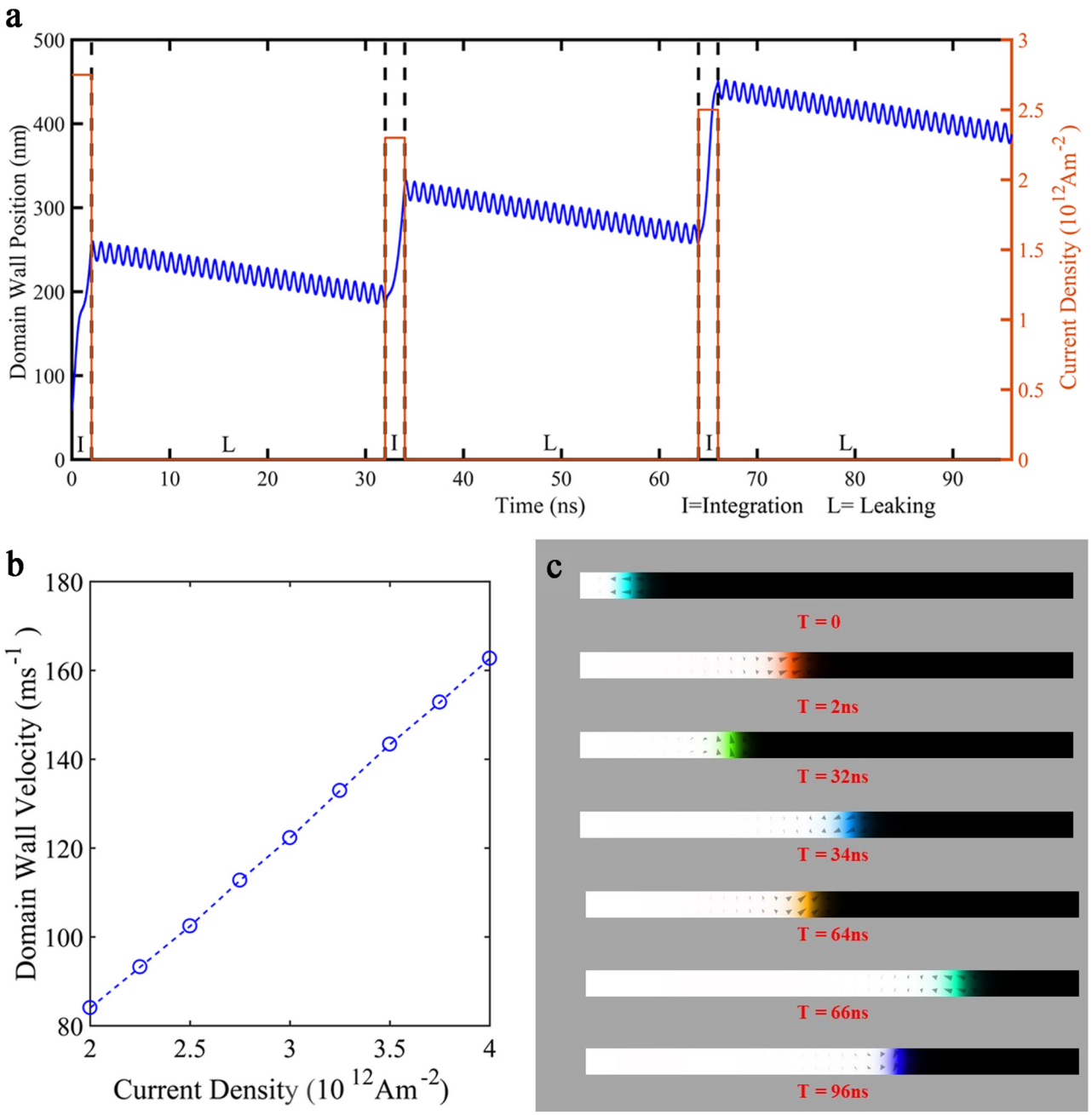

FIG. 4. Leaking and integration of the DW-MTJ neuron. (a) Time vs. DW position plot for three consecutive 2 ns long current pulses of magnitude 2.75, 2.3, and 2.5×10^{12} A/m^2, respectively, separated by 30 ns leaking periods. During the current pulse periods, integration functionality is taking place. The leaking functionality resulting from the magnetic field created by the fixed ferromagnet causes precessional DW motion. (b) Current density vs. DW velocity. (c) Mumax3 snapshots of the integration and leaking at the times noted by dashes in the plot of (a). (Multimedia view).

C. Integration

In order to integrate the input current and eventually cause the neuron to fire, current applied to the DW track above the $\sim 2 \times 10^{12}$ A/m^2 threshold current overcomes the leaking field and causes the DW to shift in the $+x$ direction. Figure 4 therefore demonstrates the ability of the DW-MTJ neuron to both integrate and leak without any external circuitry. As the integration is significantly faster than the leaking, this artificial neuron can continually integrate infrequent input signals that push the DW further and further in the $+x$ direction. This can be seen further in the multimedia view of Fig. 4.

D. Firing

In the firing operation, the neuron generates an output spike while resetting all the neurons in the same layer to enforce a refractory period during which these neurons cannot fire. The DW-MTJ achieves this through use of the MTJ formed by the track, tunnel barrier, and pinned ferromagnet above the track as shown in Fig. 3(a). When the DW moves sufficiently in the $+x$ direction such that the magnetization direction of both the DW track and the pinned ferromagnet is in the $+z$-direction, the MTJ resistance is switched from high to low. This resistance switching can generate an output firing spike and be used as an output signal or

propagate to cascaded synapses. In addition, the output firing spike can also trigger a peripheral circuit that fires the neuron by sending a current in the direction opposite to the integrating current. This firing current, in concert with the leaking magnetic field, rapidly resets the neurons to prepare for the next set of inputs from the synapses.

IV. LATERAL INHIBITION

In neuroscience, the relation between two neurons can be such that the excitation of one neuron inhibits the other neuron from firing[41]—the mechanism is referred to as lateral inhibition. For neighboring ferromagnetic tracks above a shared fixed ferromagnet as depicted in Fig. 3(b), the motion of a DW can be inhibited by the stray fields from neighboring neurons. In particular, each ferromagnetic track creates a dipolar field that attempts to orient neighboring neurons antiparallel (repulsive coupling). This pushes a slower neighboring DW in the opposite direction and thus laterally inhibits the slower neuron. To induce repulsive coupling, the neighboring tracks should be polarized as shown in Fig. 5.

The DW-MTJs provide lateral inhibition with the DW velocity of a particular ferromagnetic track dependent on the current flowing through neighboring tracks. For two neighboring ferromagnetic tracks, the track carrying a higher current acts as the inhibiting neuron and the track with the lesser current acts as the inhibited neuron. The relationship between the DW velocity of a particular track with its neighboring track current density is shown in Fig. 6. For this example, neuron1 inhibits neuron2 when current through neuron1 increases beyond 1.5×10^{12} A/m^2.

To demonstrate this property, in Fig. 7, we have simulated two ferromagnetic tracks separated by 6 nm along the y direction, with two different sets of applied current densities. For the first set of current densities (situation a), neuron1 is inhibiting neuron2 by carrying a larger current. For the second set (situation b), the inhibitory property of neuron1 is diminished by applying no current through it. Thus, due to the lack of inhibition in situation b, neuron2's DW can reach the right end point of the track earlier than in situation a. To provide insight regarding the transient inhibitory properties, the DW positions are plotted in Fig. 8(a). The relatively slower motion of neuron2 in situation a as compared to situation b is a clear indication of lateral inhibition. This is the first demonstration of intrinsic lateral inhibition between artificial neurons without external circuitry.

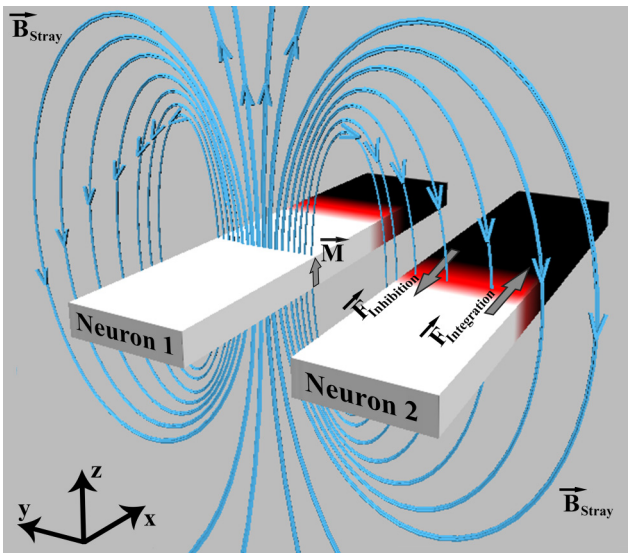

FIG. 5. The stray magnetic field from neuron 1 pushes the DW of neuron 2 in the $-x$ direction, impeding the $+x$-directed integration. Neuron 2 also produces stray magnetic fields that influence neuron 1, but are not shown in this figure.

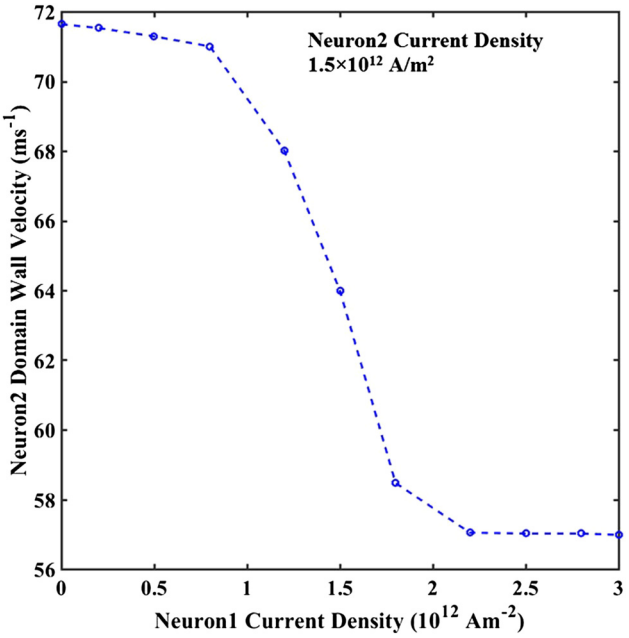

FIG. 6. Inhibitory relation between two neurons. A 1.5×10^{12} A/m^2 fixed current density is applied through ferromagnetic neuron2 while the current density through neuron1 is varied between 0 and 3×10^{12} A/m^2. When neuron1's current density increases beyond the neuron2's current density, neuron2's DW velocity is significantly reduced.

V. WINNER-TAKE-ALL HANDWRITTEN DIGIT RECOGNITION

To verify the effectiveness of this system, the well-known handwritten digit recognition test is run with micromagnetic simulation. 8×8 resolution handwritten digits are sourced from the scikit-learn database and run through a synapse crossbar, with the first neuron to fire determining the classification of the digit. Overall, the system identifies the digits with a 94% accuracy over 100 samples.

A. Handwritten digit recognition task

In order to evaluate the behavior of the proposed spintronic neurons in a larger nanoelectronic environment, an actual data science task was presented to a simulated memristive crossbar of generic nanodevice synapses. The chosen data science task was the digits database imported from the Python library scikit-learn, which is a downsampled version of the classic MNIST database (64 instead of 784 input features). The database consists of 1797 total samples of handwritten digits in 10 separated classes. Following the setup

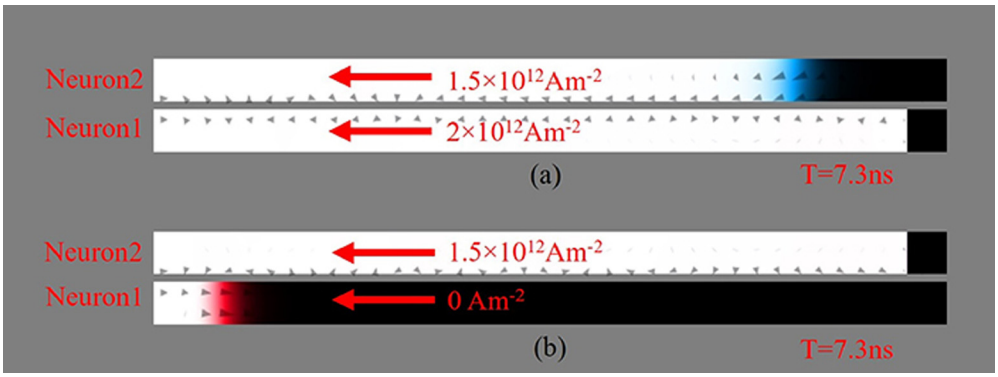

FIG. 7. Micromagnetic simulation snapshots of two z-axis-polarized ferromagnetic tracks separated by 6 nm along y-direction that provide lateral inhibition. For situation (a), we apply 1.5×10^{12} and 2×10^{12} A m^{-2} along the top (neuron2) and bottom (neuron1) tracks, respectively. For situation (b), 1.5×10^{12} and 0 A m^{-2} current densities are applied, respectively. The snapshots are taken 7.3 ns after the application of current. In situation (a), the top track is inhibited by the bottom track because of higher current through the bottom track. In this case, the bottom track DW pushes the top track DW in the $-x$ direction. In situation (b), the top track is not inhibited by bottom track due to the absence of current through bottom track, thus enabling the DW to reach the right end point earlier than in situation (a).

given in Ref. 49, the simulated crossbar learns using a binary adaptation of the classic Widrow-Hoff learning algorithm;[50] the analog input features are mapped to the voltage domain and presented in a sign-symmetric fashion such that each component of the input X_i feeds into a positive line X_{i+} and a negative line X_{i-}. Considering the bias lines and the ten different classes of outputs, the simulated crossbar has a dimensionality of 130 input wires and ten output wires.

Before learning, the database is separated into a training set of 1300 samples and a testing set of 497 samples, which are never mixed. During a separated training phase consisting of ten epochs of shuffled presentation of the training dataset, the conductance of all synapses in the array is progressively adapted in order to minimize training error. During the testing phase, the trained crossbar performs inference. Electrically, the unknown digits are presented to

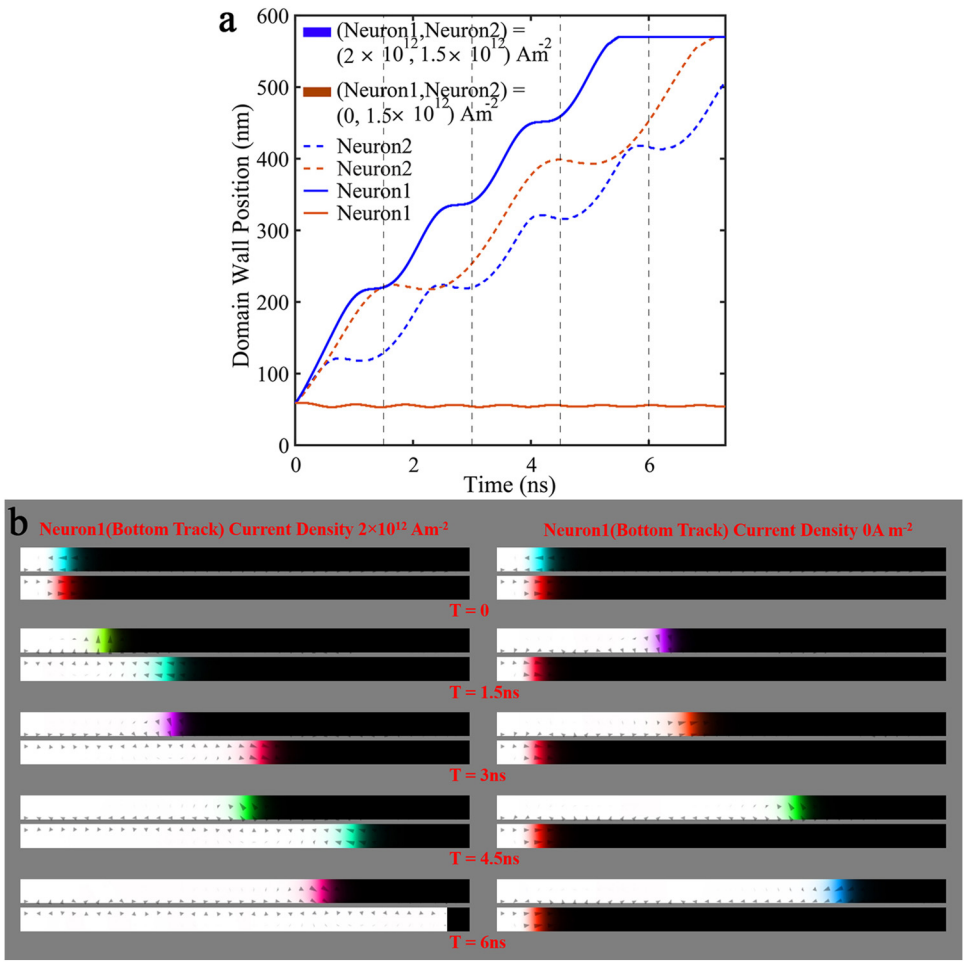

FIG. 8. (a) Time vs. DW position of laterally inhibited neurons, demonstrating the ability of neuron1 to inhibit the motion of neuron2. (b) Snapshots of the DW propagation at an interval of 1.5 ns for the two current density sets. Each set of images corresponds to a time marked by the dashed lines in (a).

the input wires and ten output currents are automatically obtained at the output.

B. Micromagnetic recognition results

Large-scale micromagnetic simulations of an array of ten of these neurons are simulated to demonstrate the effectiveness of this neuron for neuromorphic applications. Each of the ten neurons represents the recognition of one digit, and their 20 nm separation is close enough for lateral inhibition to occur. While this 20 nm separation represents an aggressive scaling target, it can be achieved using high-resolution lithography processing;[51,52] magnetic tunnel junctions have been patterned down to 20 nm diameter with on/off ratios greater than 100%,[53] and block copolymer methods have resulted in close-packed magnetic tunnel junction disks with 13 nm separation.

The lateral inhibition, in this system, implements a "winner take all" functionality—if one of the neurons has a higher input current than the others, the current flowing through the other neurons is insufficient to shift the DW against the spin transfer torque. This ensures that only one neuron is able to fire at a time. To test the effectiveness of this system, we apply the output currents attained from the method described above. Before these current density values are used, they are normalized to the acceptable neuron current range of 1.5×10^{12} to 4×10^{12} A/m^2. After normalization, the currents can be applied to each of the ten devices as the integrating input current. Once the DW has shifted along 95% of the track and across the MTJ, the MTJ resistance switches and the neuron fires. The firing mechanism sends a current to reset the neurons as soon as one DW position traverses the MTJ. Finally, there is a leaking phase at the end of the simulation, to demonstrate the leaking ability of the device, which along with the reset current represents the refractory period. The application of each input number lasts a constant time of 30 ns, with the time of the leaking phase varying depending on the time of the integrating phase.

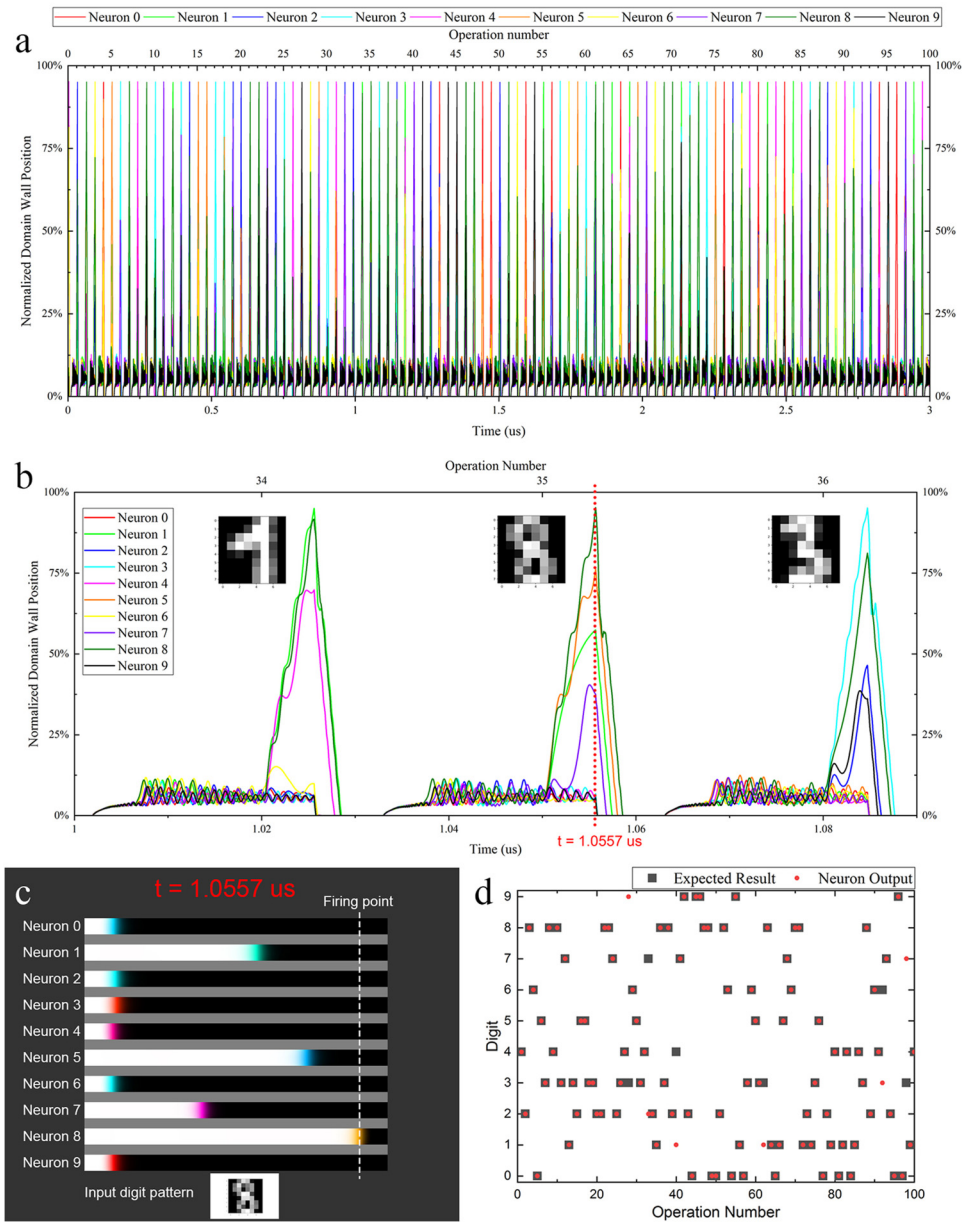

FIG. 9. Simulation results of laterally-inhibited ten-neuron winner-take-all output layer. (a) Graph result of the classification simulation. As each simulation lasts for 30 ns, 100 cycles have been plotted, with each spike representing one digit. Figs. S2–S5 in the supplementary material provide a more detailed picture of the behavior, including an example of a neuron failure. (b) Zoomed in representation of the simulation, portraying only three cycles. The input image that was used for identification is shown beside their relative cycle. (c) Mumax3 micromagnetic simulation snapshot of the simulation. The 8×8 input image is provided below, to provide context on the handwritten digit being identified by the system. In this case, since neuron #2 fired, the system correctly identified the image. (d) Plot of expected results vs. output digit. When the output matches the input, they overlap. Every input digit data point that is visible is therefore a failed classification. In this case, there are six failures out of one hundred, displaying our 94% accuracy. [Ten-part multimedia view for (c)].

Figure 9(a) displays the results in graph form, after 100 cycles have run. The winner of each cycle can be seen by which color reaches the end of the track (in this case, the 95% mark), with each color corresponding with a neuron. For a clearer representation of three cycles, a zoomed-in version is provided in Fig. 9(b) along with the original input image in order to add context to what was being identified (see Figs. S2–S5 in the supplementary material for additional representations of these simulation results). Figure 9(c) provides a visualization of the graph data, showing a Mumax3 simulation snapshot; multimedia view is also included. This figure only represents only one cycle of graph data, at the climax of the firing phase, taken as a snapshot from video (d) of the multimedia view. As can be seen from Fig. 9(d), this system had a 94% accuracy in selecting the correct winning neuron that corresponded with the currents provided by the synapse array. Similar to other neuromorphic systems, this neuron output layer is highly tolerant to fabrication imprecision, as demonstrated through a Monte Carlo technique in Fig. S1 in the supplementary material.

VI. CONCLUSIONS

Nanodevices that intrinsically emulate neurological behaviors have the potential to enable highly efficient neuromorphic computing systems. This work therefore proposes a leaky integrate-and-fire neuron that intrinsically provides lateral inhibition. When integrated with a crossbar synapse structure, a layer of ten DW-MTJ neurons classified over 100 8×8 handwritten digits with 94% integrity. With the potential to integrate the proposed DW-MTJ neurons with previously demonstrated DW-MTJ synapses, these leaky integrate-and-fire neurons with intrinsic lateral inhibition have the potential to enable highly effective neuromorphic information processing systems. Eventually, the intrinsic inhibition properties of our devices could be used not only for efficient inference operations, but also to realize previously hardware-expensive operations such as local spike-timing dependent plasticity (STDP) learning.

SUPPLEMENTARY MATERIAL

See supplementary material for additional figures and videos of the micromagnetic simulation.

[1]V. Balasubramanian, Proc. IEEE **103**, 1346–1358 (2015).
[2]F. Akopyan, J. Sawada, A. Cassidy, R. Alvarez-Icaza, J. Arthur, P. Merolla, N. Imam, Y. Nakamura, P. Datta, G. J. Nam, B. Taba, M. Beakes, B. Brezzo, J. B. Kuang, R. Manohar, W. P. Risk, B. Jackson, and D. S. Modha, IEEE Trans. Comput. Des. Integr. Circuits Syst. **34**, 1537–1557 (2015).
[3]P. A. Merolla, J. V. Arthur, R. Alvarez-Icaza, A. S. Cassidy, J. Sawada, F. Akopyan, B. L. Jackson, N. Imam, C. Guo, Y. Nakamura, B. Brezzo, I. Vo, S. K. Esser, R. Appuswamy, B. Taba, A. Amir, M. D. Flickner, W. P. Risk, R. Manohar, and D. S. Modha, Science **345**, 668–673 (2014).
[4]T. V. Bliss and A. R. Gardner-Medwin, J. Physiol. **232**, 357–374 (1973).
[5]A. Delorme, J. Gautrais, R. Van Rullen, and S. Thorpe, Neurocomputing **26–27**, 989–996 (1999).
[6]S. Han, H. Mao, and W. J. Dally, e-print arXiv:1510.00149 (2015).
[7]D. A. Pomerleau, in *International Conference on Neural Networks* (1988), pp. 143–150.
[8]M. Fischetti, Sci. Am. **305**, 104 (2011).
[9]B. Sengupta and M. B. Stemmler, Proc. IEEE **102**, 738–750 (2014).
[10]G. F. D. Betta, S. Graffi, Z. M. Kovacs, and G. Masetti, IEEE Trans. Circuits Syst. II Analog Digit. Signal Process. **40**, 206 (1993).
[11]H. P. Graf, L. D. Jackel, and W. E. Hubbard, IEEE J. Sel. Top. Quantum Electron. **3**, 41–49 (1988).
[12]A. Masaki, Y. Hirai, and M. Yamada, IEEE Circuits Devices Mag. **6**, 12–17 (1990).
[13]J. J. Yang, J. Borghetti, D. Murphy, D. R. Stewart, and R. S. Williams, Adv. Mater. **21**, 3754–3758 (2009).
[14]L. O. Chua, IEEE Trans. Circuit Theory **18**, 507–519 (1971).
[15]D. B. Strukov, G. S. Snider, D. R. Stewart, and R. S. Williams, Nature **453**, 80–83 (2008).
[16]M. Chu, B. Kim, S. Park, H. Hwang, M. Jeon, B. H. Lee, and B. G. Lee, IEEE Trans. Ind. Electron. **62**, 2410–2419 (2015).
[17]M. Al-Shedivat, R. Naous, G. Cauwenberghs, and K. N. Salama, IEEE J. Emerg. Sel. Top. Circuits Syst. **5**, 242–253 (2015).
[18]G. Indiveri, B. Linares-Barranco, R. Legenstein, G. Deligeorgis, and T. Prodromakis, Nanotechnology **24**, 384010 (2013).
[19]G. L. Gerstein and B. Mandelbrot, Biophys. J. **4**, 41–68 (1964).
[20]H. Markram, M. Toledo-Rodriguez, Y. Wang, A. Gupta, G. Silberberg, and C. Wu, Nat. Rev. Neurosci. **5**, 793 (2004).
[21]T. C. Jacob, S. J. Moss, and R. Jurd, Nat. Rev. Neurosci. **9**, 331 (2008).
[22]D. Feldmeyer, G. Qi, V. Emmenegger, and J. F. Staiger, Neuroscience **368**, 132–151 (2018).
[23]A. Sengupta and K. Roy, Appl. Phys. Rev. **4**, 041105 (2017).
[24]J. Grollier, D. Querlioz, and M. D. Stiles, Proc. IEEE **104**, 2024–2039 (2016).
[25]A. Sengupta and K. Roy, IEEE Trans. Circuits Syst. I **63**, 2267–2277 (2016).
[26]A. Sengupta, Y. Shim, and K. Roy, IEEE Trans. Biomed. Circuits Syst. **10**, 1152–1160 (2016).
[27]A. Sengupta, S. H. Choday, Y. Kim, and K. Roy, Appl. Phys. Lett. **106**, 143701 (2015).
[28]G. Srinivasan, A. Sengupta, and K. Roy, in *Proceedings of DATE* (2017), pp. 530–535.
[29]A. Jaiswal, S. Roy, G. Srinivasan, and K. Roy, IEEE Trans. Electron Devices **64**, 1818–1824 (2017).
[30]A. Jaiswal, A. Agrawal, P. Panda, and K. Roy, e-print arXiv:1705.06942 (2017).
[31]A. Sengupta, P. Panda, P. Wijesinghe, Y. Kim, and K. Roy, Sci. Rep. **6**, 1–9 (2016).
[32]J. A. Currivan-Incorvia, S. Siddiqui, S. Dutta, E. R. Evarts, J. Zhang, D. Bono, C. A. Ross, and M. A. Baldo, Nat. Commun. **7**, 10275 (2016).
[33]J. A. Currivan, Y. Jang, M. D. Mascaro, M. A. Baldo, and C. A. Ross, IEEE Magn. Lett. **3**, 3000104 (2012).
[34]A. Roohi, R. Zand, and R. F. Demara, IEEE Trans. Magn. **52**, 1–7 (2016).
[35]S. Lequeux, J. Sampaio, V. Cros, K. Yakushiji, A. Fukushima, R. Matsumoto, H. Kubota, S. Yuasa, and J. Grollier, Sci. Rep. **6**, 31510 (2016).
[36]S. Dutta, S. A. Siddiqui, F. Buttner, L. Liu, C. A. Ross, and M. A. Baldo, IEEE/ACM Int. Symp. Nanoscale Archit. (NANOARCH) (2017), pp. 83–88.
[37]Q. Dong, K. Yang, L. Fick, D. Blaauw, and D. Sylvester, Proc. IEEE Int. Symp. Circuits Syst. **4**, 0–3 (2017).
[38]P. Sheridan, W. Ma, and W. Lu, in *Proceedings of IEEE International Symposium Circuits and Systems* (2014), pp. 1078–1081.
[39]A. N. Burkitt, Biol. Cybern. **95**, 97–112 (2006).
[40]S. H. Jo, T. Chang, I. Ebong, B. B. Bhadviya, P. Mazumder, and W. Lu, Nano Lett. **10**, 1297–1301 (2010).
[41]S. ichi Amari, Biol. Cybern. **27**, 77–87 (1977).
[42]E. Meir, G. Von Dassow, E. Munro, and G. M. Odell, Curr. Biol. **12**, 778–786 (2002).
[43]Z. H. Mao and S. G. Massaquoi, IEEE Trans. Neural Netw. **18**, 55–69 (2007).
[44]J. Lazzaro, S. Ryckebusch, M. A. Mahowald, and C. A. Mead, in *Adv. Neural Inf. Process Syst* (1988), pp. 703–711.
[45]A. V. Khvalkovskiy, V. Cros, D. Apalkov, V. Nikitin, M. Krounbi, K. A. Zvezdin, A. Anane, J. Grollier, and A. Fert, Phys. Rev. B Condens. Matter Mater. Phys. **87**, 2–6 (2013).
[46]S. Emori, U. Bauer, S. M. Ahn, E. Martinez, and G. S. D. Beach, Nat. Mater. **12**, 611–616 (2013).
[47]A. Vansteenkiste, J. Leliaert, M. Dvornik, M. Helsen, F. Garcia-Sanchez, and B. Van Waeyenberge, AIP Adv. **4**, 107133 (2014).

[48]X. Hu, M. J. Schultis, M. Kramer, A. Bagla, A. Shetty, and J. S. Friedman, IEEE Trans. Circuits Syst. I 2018, 99.
[49]C. Bennett, J. E. Lorival, F. Marc, T. Cabaret, B. Jousselme, V. Derycke, J. O. Klein, and C. Maneux, "Multiscaled simulation methodology for neuro-inspired circuits demonstrated with an organic memristor," IEEE Trans. Multi-Scale Comput. Syst. (published online).
[50]B. Widrow and M. A. Lehr, Proc. IEEE **78**, 1415–1442 (1990).
[51]J. A. Currivan, S. Siddiqui, S. Ahn, L. Tryputen, G. S. D. Beach, M. A. Baldo, and C. A. Ross, J. Vac. Sci. Technol. B Nanotechnol. Microelectron. Mater. Process. Meas. Phenom. **32**, 021601 (2014).
[52]K. Tu, E. Fernandez, H. Almasi, W. Wang, D. N. Otero, K. Ntetsikas, D. Moschovas, A. Avgeropoulos, and C. A. Ross, Nanotechnology **29**, 275302 (2018).
[53]L. Xue, A. Kontos, C. Lazik, S. Liang, and M. Pakala, IEEE Trans. Magn. **51**, 18–20 (2015).